A Nonlinear Guided Filter for Polarimetric SAR Image Despeckling

Xiaoshuang Ma, Penghai Wu, *Member, IEEE*, and Huanfeng Shen, *Senior Member, IEEE*

***Abstract*— Despeckling is a fundamental preprocessing step for applications using polarimetric synthetic aperture radar data in most cases. In this paper, a guided filter with nonlinear weight kernels and adaptive filtering windows is presented for PolSAR image despeckling, in which the guidance image is constructed by a weighted average using the statistical traits of the speckled image. The output result is then estimated by another weighted average, with the aid of the fully polarimetric information from both the guidance image and the speckled image. In the experimental part, the filtering results obtained with both simulated and real PolSAR images reveal the positive performance of the proposed method in both reducing speckle and retaining details, when compared with some of the state-of-the-art algorithms. Furthermore, the relatively low computational complexity is another strength of the proposed method.**

***Index Terms*— Guided filter, polarimetric synthetic aperture radar (PolSAR), speckle filtering, Wishart distribution.**

I. Introduction

AS AN advanced form of synthetic aperture radar (SAR), polarimetric SAR systems are capable of emitting and receiving fully polarized radar waves to characterize observed targets, together with the all-weather, day-and-night imaging capabilities, resulting in their wide use in many areas. However, PolSAR data are inherently affected by speckle noise, which degrades the quality of PolSAR images and complicates the task of image interpretation. As a result, despeckling is a fundamental preprocessing step for applications using PolSAR data in most cases.

The studies of PolSAR filters can be traced back to the beginning of the 1990s. During the last three decades, many different PolSAR filtering techniques have been developed. In [1], we made a broad view of the existing PolSAR filters, which can be generally categorized into five classes: 1) local filters; 2) nonlocal means (NLM)-based methods; 3) partial differential equation-based methods; 4) variational methods; and 5) machine learning-based methods. One of the classical PolSAR filters is the refined Lee filter [2], which was developed based on the linear minimum mean-squared error (LMMSE) estimator originally designed for single-polarization SAR image despeckling [3]. The refined Lee filter has opened up an important branch of filtering methods based on the LMMSE estimator [4], [5]. The core issue of these methods is to investigate means of selecting similar pixels to ensure stationarity of the scene. Lee *et al.* [6] generalized the idea of the sigma filter [7] to select similar pixels in a local window, without the deficiencies of the original sigma filter in underestimating and blurring strong targets; in the meantime, the bias introduced by the original sigma range is also compensated in the improved sigma filter. Recently, Lee *et al.* [8] proposed a new algorithm to further amend the improved sigma filter by a more sophisticated strategy of detecting strong point targets and selecting similar pixels. Other traditional PolSAR filters include, but are not limited to, the segmentation-based filter [9], the bilateral filter [10], and the speckle model-based filter [11]. In recent years, the NLM filter [12]–[14], which was originally designed for digital image denoising [15], has been a hot topic in PolSAR image despeckling. Differing from the traditional methods, the NLM filter not only searches and compares the values in a single point in a small local window, but also the geometrical configuration in the whole image, so that it can obtain more robust results. Anisotropic diffusion-based filters [16], [17], variational-based filters [18]–[20], and the simultaneous sparse coding (SSC)-based filter [21] have also been developed in recent years.

He *et al.* [22] introduced a new concept of guided filtering for digital image denoising, which involves filtering the input image with the aid of a guidance image. The guidance image can be the noisy input image or an explicit one. A linear relationship between the noisy image and guidance image is assumed, and the guidance image guides the structure-transferring filter operation. Recently, Ni and Gao [23] applied the idea of the guided filter to process single-polarization SAR images. Differing from the original linearly guided filter, Ni and Gao [23] constructed a nonlinear weight kernel, the expression of which is deduced within the Bayesian NLM framework. Positive despeckling results for the SAR guided filter have been reported when compared with some of the other advanced methods.

Inspired by the idea of the SAR guided filter proposed in [23], a nonlinear guided filter with adaptive filtering windows is presented in this paper for the despeckling of fully

Manuscript received July 17, 2018; revised September 6, 2018; accepted September 8, 2018. This work was supported in part by the National Natural Science Foundation of China under Grant 41701390 and Grant 61671334 in part by the Natural Science Foundation of Anhui Province under Grant 1808085QD108, and in part by the Open Fund for Discipline Construction of the Institute of Physical Science and Information Technology, Anhui University. (*Corresponding author: Penghai Wu.*)

X. Ma is with the Department of Resources and Environmental Engineering, Anhui University, Hefei 230601, China (e-mail: mxs.88@whu.edu.cn).

P. Wu is with the Institute of Physical Science and Information Technology, Anhui University, Hefei 230601, China (e-mail: wuph@ahu.edu.cn).

H. Shen is with the Department of Resource and Environmental Sciences, Wuhan University, Wuhan 430079, China (e-mail: shenhf@whu.edu.cn).

Color versions of one or more of the figures in this paper are available online at http://ieeexplore.ieee.org.

Digital Object Identifier 10.1109/TGRS.2018.2870188

polarimetric SAR images. The main idea behind the proposed method is to guide the despeckling operation by combining the fully polarimetric information from both the speckled image and a guidance image, where the guidance image is constructed by a prefiltering process using the information of the speckled image.

The remainder of this paper is organized as follows. Section II introduces the statistical models of PolSAR data and the idea of the guided filter. In Section III, the proposed PolSAR nonlinear guided filter (PNGF) is presented. Then, in Section IV, we describe the experiments conducted on both simulated and real PolSAR images to validate the performance of the proposed method. Finally, the conclusion is provided in Section V.

II. Statistical Models of PolSAR Data and the Guided Filter

A. Statistical Models of PolSAR Data

A fully polarimetric SAR system measures the complex scattering matrix of a medium with quad-polarizations. For the reciprocal backscattering case, the backscattered radar signal from each cell of the PolSAR system can be characterized by the following scattering vector:

$$\boldsymbol{v} = (S_{\mathrm{HH}}, \sqrt{2}S_{\mathrm{HV}}, S_{\mathrm{VV}})^T \tag{1}$$

where S_{HV} denotes the scattering element of the vertical transmitting and horizontal receiving polarizations, with the combination of the amplitude $|S_{\mathrm{HV}}|$ and the phase ϕ_{HV}: $S_{\mathrm{HV}} = |S_{\mathrm{HV}}|e^{j\phi_{\mathrm{HV}}}$. The other elements in the scattering matrix are similarly defined. SAR data are frequently multilook processed for speckle reduction and data compression by averaging several neighboring single-look pixels. Multilook polarimetric data are often represented by a polarimetric covariance matrix, which is generated from the outer product of the target vector with its conjugate transpose. The polarimetric covariance matrix is a Hermitian positive definite matrix.

Most of the PolSAR filters were derived based on the assumption of "fully developed speckle," which has the following properties [24]: 1) a large number of scatterers in a resolution cell of a homogeneous medium; 2) the range distance is much larger than the radar wavelength; and 3) the surface is much rougher on the scale of the radar wavelength. It has been proven that [25], for fully developed speckle, the L-look covariance matrix C_L follows a complex Wishart distribution:

$$P(\mathbf{C}_L|\mathbf{Z}) = \frac{L^{qL}|\mathbf{C}_L|^{L-q}\exp\{-L\mathrm{Tr}(\mathbf{Z}^{-1}\mathbf{C}_L)\}}{Q(L,q)|\mathbf{Z}|^L} \tag{2}$$

with

$$Q(L,q) = \pi^{q(q-1)/2}\prod_{i=1}^{q}\Gamma(L-i+1) \tag{3}$$

where $\mathrm{Tr}(\cdot)$ and $|\cdot|$ are, respectively, the trace operator and the determinant operator. $\mathbf{Z}$ is the population covariance matrix. Parameter $q = 3$ is the dimension of the polarimetric covariance matrix.

Compared with single-polarization SAR data, the speckle model of fully PolSAR data is much more complex. Speckle noise not only appears in the intensity image of each polarization, but also in the complex cross-product terms. It has been found that the diagonal terms of the polarimetric covariance matrix can be characterized by a multiplicative noise model, while the off-diagonal terms have the characteristics of a combined multiplicative and additive noise model [26]. Lee *et al.* [2] proposed the PolSAR filtering principle, i.e., to preserve the polarimetric properties, all the terms of the matrix should be filtered in the same way; in other words, filtered by the same amount.

B. Guided Filter

The guided filter [22] assumes that the relationship between the guidance image G and the filtering result R can be described by the following linear model:

$$R_i = a_x G_i + b_x \quad \forall i \in \Delta x \tag{4}$$

where Δx is a local window centered at pixel x and a_x and b_x are linear coefficients which are constant for the window Δx and are deduced by means of linear ridge regression [27] as follows:

$$a_x = \sum_{j\in\Delta x} A_{x,j}(G)\cdot U_j \tag{5}$$

$$b_x = \sum_{j\in\Delta x} B_{x,j}(G)\cdot U_j \tag{6}$$

where U denotes the noisy input image. It can be seen that terms $A_{x,i}(G)$ and $B_{x,i}(G)$ depend only on the guidance image and a_x and b_x are computed as the weighted average of the pixels in Δx in the input image. From (5) and (6), we can rewrite (4) as follows:

$$R_i = \sum_{j\in\Delta x}[A_{x,j}(G_i)\cdot G_i + B_{x,j}(G_i)]U_j \quad \forall i \in \Delta x. \tag{7}$$

To solve the problem of multiple estimations for the same pixel R_i under different overlapping windows, all possible values are averaged. Therefore, we can deduce (7) as follows:

$$R_i = \frac{1}{|\Delta x|}\sum_{i\in\Delta x}\sum_{j\in\Delta x}[A_{x,j}(G_i)\cdot G_i + B_{x,j}(G_i)]U_j. \tag{8}$$

To avoid oversmoothing and ease computational burden, one can directly use the noisy image U as the guidance image G. Then, due to the symmetry of the box window, (8) can be rewritten as [23]

$$R_i = \frac{1}{|\Delta i|}\sum_{x\in\Delta i}\sum_{j\in\Delta x}[A_{x,j}(U_i)\cdot U_i + B_{x,j}(U_i)]U_j \tag{9}$$

where Δi is a local window centered at pixel i.

III. PolSAR Nonlinear Guided Filter

A. Extension of Guided Filter to PolSAR Despeckling

He *et al.* [22] proposed that the guided filter can be straightforwardly applied to denoise color or multichannel images, which is given by

$$\boldsymbol{R}_i^y = \boldsymbol{a}_x^y \boldsymbol{U}_i^y + \boldsymbol{b}_x^y \quad \forall i \in \Delta x \tag{10}$$

where superscript y denotes the index of image channel. Then, as (4)–(9), we can easily derive that

$$\boldsymbol{R}_i^y = \frac{1}{|\Delta i|}\sum_{x\in\Delta i}\sum_{j\in\Delta x}\left[A_{x,j}\left(\boldsymbol{U}_i^y\right)\cdot\boldsymbol{U}_i^y + B_{x,j}\left(\boldsymbol{U}_i^y\right)\right]\boldsymbol{U}_j^y. \quad (11)$$

To simplify (11), we let the weight of pixel j in the local window of pixel x be $p_{x,j}(\boldsymbol{U}_i^y) = A_{x,j}(\boldsymbol{U}_i^y)\cdot\boldsymbol{U}_i^y + B_{x,j}(\boldsymbol{U}_i^y)$ and the weight of pixel x in the local window of pixel i be $q_{i,x} = 1/|\Delta i|$, the guided filter can be finally represented as

$$\boldsymbol{R}_i^y = \sum_{x\in\Delta i} q_{i,x}\left(\sum_{j\in\Delta x} p_{x,j}\left(\boldsymbol{U}_i^y\right)\boldsymbol{U}_j^y\right). \quad (12)$$

Clearly, we can observe from (12) that for each channel of the data, the guided filter formally consists of two weighted averaging steps: 1) the filtering result of pixel i is, in fact, the weighted average of the prefiltering output in its local window Δi and 2) the prefiltering output is in turn computed as another weighted average of the pixels in the local window Δx for each pixel in Δi, where the weight kernel $p_{x,j}(\boldsymbol{U}_i^y)$ is linear and constructed based on the guidance image (actually, the noisy image).

The guided filter is originally designed for the filtering of digital images which are contaminated by additive white noise. However, if we extend this method to process fully polarimetric SAR images, several issues are worthy of notice.

1) First of all, when filtering the color or multichannel digital images, different values of the weight term $p_{x,j}(\boldsymbol{U}_i^y)$ are deployed for different channels in [22]. However, this is not feasible for PolSAR data. As we pointed out in Section II, a main principle of PolSAR despeckling is to filter each term of the polarimetric covariance matrix by the same amount to preserve the polarimetric properties.
2) The weight kernels should be derived based on the statistical trait of the speckle, rather than simply employed the weights in the original guided filter.

To cope with the despeckling problem of single-polarization SAR image, Ni and Gao [23] proposed to generalize the linear guided filter into a nonlinear filter, and take both the speckled image and the prefiltered image into account when calculating the weights in the second averaging step.

In this paper, adhered to the above ideas and motivated by the work in [22] and [23], a nonlinear guided filter with adaptive filtering windows is developed for PolSAR image despeckling. This filtering method consists of two weighted averaging steps: 1) in the first step, a prefiltered image is constructed by a weighted average with a nonlinear weight kernel using the information of the original speckled image and 2) in the second step, the output result of each pixel is estimated by another weighted average using the information from both the prefiltered image and the speckled image. The proposed PNGF method is formulated as follows:

$$\boldsymbol{C}_i = \sum_{x\in\Delta i} q_{i,x}(\boldsymbol{S},\boldsymbol{F})\boldsymbol{S}_x \quad (13)$$

with

$$\boldsymbol{F}_x = \sum_{j\in\Delta x} p_{x,j}(\boldsymbol{S})\boldsymbol{S}_j \quad (14)$$

where $\boldsymbol{S}$, $\boldsymbol{F}$, and $\boldsymbol{C}$ are, respectively, the polarimetric covariance matrices of the speckled image, the prefiltered image, and the output image.

The main idea behind the PNGF method is, in the step of calculating the prefiltered image $\boldsymbol{F}$ by (14), only the statistical traits in the speckled image $\boldsymbol{S}$ can be used. Once the prefiltered image is constructed, the basic estimation of each pixel x in the local window of pixel i is obtained. To some degree, this prefiltered image acts as the role of a guidance image. Then, with the aid of both the speckled image and guidance image, a refined weighted average of the pixels in the local window is taken to estimate the final result of pixel i.

B. Construction of Nonlinear Weight Kernels

Clearly, the main issue with the proposed PNGF method is the construction of the weight kernels in (13) and (14). In this paper, as did in [23], we employ nonlinear weight kernels, as follows:

$$p_{x,j}(\boldsymbol{S}) = \exp\left\{-\left[\frac{D\left(\boldsymbol{C}_x^* = \boldsymbol{C}_j^*\middle|\boldsymbol{S}_x,\boldsymbol{S}_j\right)}{t1}\right]^2\right\} \quad (15)$$

$$q_{i,x}(\boldsymbol{S},\boldsymbol{F}) = \exp\left\{-\left[\frac{D\left(\boldsymbol{C}_i^* = \boldsymbol{C}_x^*\middle|\boldsymbol{S}_i,\boldsymbol{S}_x,\boldsymbol{F}\right)}{t2}\right]^2\right\} \quad (16)$$

where $\boldsymbol{C}^*$ denotes the covariance matrices of the noise-free image, $t1$ and $t2$ are two normalization parameters, and the numerators inside the weight kernels denote the similarity between two pixels, given the speckled image $\boldsymbol{S}$ and the prefiltered image $\boldsymbol{F}$. The weight kernels of the proposed method are similar to those of the NLM filter: the more similar the pixels, the higher they have weights.

The question of constructing the nonlinear weight kernels now comes down to measuring the similarity of two pixels, given the speckled image and the prefiltered image. First, for (15), the numerator denotes the similarity between two pixels, given only the speckled image $\boldsymbol{S}$. In this research, we deploy the Wishart likelihood-ratio test statistic [28] to calculate this term. We assume that the independent 3×3 Hermitian positive definite matrices (covariance matrices) $\boldsymbol{X}$ and $\boldsymbol{Y}$ are complex Wishart distributed, i.e., $\boldsymbol{X}\in W_c(3,n,\Sigma_x)$ with $\Sigma_x^{\wedge} = 1/n\boldsymbol{X}$ and $\boldsymbol{Y}\in W_c(3,m,\Sigma_y)$ with $\Sigma_y^{\wedge} = 1/m\boldsymbol{Y}$, where $m = n$, which is the number of looks. We consider the null hypothesis, H_0: $\Sigma_x = \Sigma_y$, which states that the two matrices are equal, against the alternative hypothesis, H_1: $\Sigma_x \neq \Sigma_y$. If H_0 hypothesis is true, the Wishart likelihood-ratio test statistic can be deduced as follows [28]:

$$Q = \frac{(n+m)^{3(n+m)}}{n^{3n}m^{3m}}\frac{|\boldsymbol{X}|^m|\boldsymbol{Y}|^n}{|\boldsymbol{X}+\boldsymbol{Y}|^{m+n}}. \quad (17)$$

Taking the logarithm of (17) and discarding the constant terms, the numerator of (15) can be calculated as follows:

$$D\left(\boldsymbol{C}_x^* = \boldsymbol{C}_j^*\middle|\boldsymbol{S}_x,\boldsymbol{S}_j\right) = 6\ln 2 + \ln|\boldsymbol{S}_x| + \ln|\boldsymbol{S}_j| - 2\ln|\boldsymbol{S}_x+\boldsymbol{S}_j|. \quad (18)$$

It can be proven that this term is nonpositive, and the more similar the two pixels, the closer this term is to zero.

It needs to be noted that the likelihood-ratio test in (18) involves the matrix logarithm, which means that the involved matrices have to be full rank ($|\mathbf{C}| \neq 0$). However, when the number of looks is small with respect to the dimension of the covariance matrix ($L < 3$), and the resolution cell contains a dominant scatterer (for instance, strong returns from point targets) with one dominant scattering mechanism, the covariance matrix $\mathbf{C}$ could be singular ($|\mathbf{C}| = 0$), which can produce numerical instability in the filtering process. In order to avoid numerical problems, we employ a preprocessing step before the filtering, as in [14]. When calculating (18), we transform the covariance matrix to ensure that it is full rank. Transformed matrix $\boldsymbol{T}$ is denoted by

$$\forall k1, \boldsymbol{T}_{k1,k1} = \mathbf{C}_{k1,k1}; \quad \forall k1 \neq k2, \boldsymbol{T}_{k1,k2} = \gamma\, \mathbf{C}_{k1,k2} \tag{19}$$

where $k1$ and $k2$ are the indices of the elements of the matrix and $\gamma = \min(L/3, 1)$. This step only rescales the off-diagonal terms of $\mathbf{C}$, and the diagonal terms are not changed (i.e., the intensity is not changed). It was proven in [14] that the transformed data by (19) can still be modeled by the Wishart distribution defined in (2), and the likelihood-ratio test is still valid for the rescaled data.

From the aspect of probability statistics, the similarity measure in (16) can be rewritten as

$$D\big(\boldsymbol{C}_x^* = \boldsymbol{C}_j^* \big| \boldsymbol{S}_x, \boldsymbol{S}_j, \boldsymbol{F}\big) = P\big(\boldsymbol{C}_x^* = \boldsymbol{C}_j^* \big| \boldsymbol{S}_x, \boldsymbol{S}_j, \boldsymbol{F}\big). \tag{20}$$

Under a Bayesian framework, in the absence of any information on $P(\boldsymbol{S}_x, \boldsymbol{S}_j)$, and assuming that the event $P(\boldsymbol{C}_x^* = \boldsymbol{C}_j^* | \boldsymbol{S}_x, \boldsymbol{S}_j)$ is independent of the guidance image $\boldsymbol{G}$, then the following relation holds:

$$D\big(\boldsymbol{C}_i^* = \boldsymbol{C}_x^* \big| \boldsymbol{S}_i, \boldsymbol{S}_x, \boldsymbol{F}\big) = P\big(\boldsymbol{C}_i^* = \boldsymbol{C}_x^* \big| \boldsymbol{S}_i, \boldsymbol{S}_x\big) \times P\big(\boldsymbol{C}_i^* = \boldsymbol{C}_x^* \big| \boldsymbol{F}\big). \tag{21}$$

Clearly, the first term of the right-hand side of the above equation reflects the likelihood of having identical noise-free values with respect to the observed speckled image, which can be directly calculated by the means in (18). Meanwhile, the second term is calculated from the guidance image and considers its pixel values as the "true" parameters of the noise generative model. By considering the fully polarimetric information of both the speckle image and guidance image, the weights in the final filtering step are refined.

For the calculation of the second term of (21), we use the Kullback–Leibler divergence, which can characterize the discrepancy between two probability distributions. For PolSAR data, the symmetric Kullback–Leibler divergence between two zero-mean complex circular Gaussian distributions is given by [10]

$$P\big(\boldsymbol{C}_i^* = \boldsymbol{C}_x^* \big| \boldsymbol{F}\big) = \mathrm{tr}[(\boldsymbol{F}_i)^{-1}\boldsymbol{F}_x + \boldsymbol{F}_i(\boldsymbol{F}_x)^{-1}] - 6 \tag{22}$$

where $P(\boldsymbol{C}_i^* = \boldsymbol{C}_x^* | \boldsymbol{F}) \geq 0$, and the more similar the two pixels, the closer this term is to zero.

It should be pointed out here that as in the proposed PNGF method, a two-step filtering strategy has also been employed in the nonlocal SAR (NL-SAR) filter proposed by Deledalle *et al.* [14]. However, the proposed filter has the following major differences and benefits with regard to the NL-SAR filter.

1) In the prefiltering step, a strategy is employed in the NL-SAR filter to select locally the best preprocessing among several scales of averaging. However, the results of a different scale of averaging are obtained mainly using the intensity information of PolSAR data. Differing from NL-SAR, the prefiltering step of the proposed method is simply a local weighted averaging step, but all polarimetric information is utilized.
2) In the final filtering step, to calculate the weights of the pixels in the searching window, only the polarimetric information of the prefiltered data is considered in the NL-SAR filter. A limit of such approach is that the pre-estimation result must be good enough to make it possible to discriminate low-contrast features; otherwise, they will be smoothed out after the second filtering step [14]. On the contrary, in the proposed method, the polarimetric information of the original speckled image is also taken into account to prevent the image from over-smoothing in the final filtering step.
3) The NL-SAR is a patch-based filter, while the proposed method is actually a pixel-based local filter, which leads to the relative lower computational complexity of the proposed method when processing the image with large size. This is further discussed in Section IV.

C. Choice of Filtering Parameters

The partial normalization parameters $t1$ and $t2$ in the weight kernel are important to control the filtering amount of the proposed method. Higher normalization parameters can result in a better performance in reducing noise, while lower parameters can result in a better performance in retaining details. In this paper, $t1$ and $t2$ are automatically determined by the "noise estimator" suggested by Canny [29]: before each weighted averaging step, a histogram of the absolute values of the similarity between any two neighboring pixels along a certain direction throughout the image is computed as (18) or (21), and $t1$ or $t2$ is set to be equal to the 80% value of its integral. By this means, $t1$ and $t2$ can be adaptively set as a larger value to better reduce the speckle, if the speckle level of the image is high, and vice versa. In practice, this value can be fine-tuned to obtain better results.

The other two parameters that need to be tuned in the PNGF method are, respectively, the sizes of the local filtering window in the prefiltering step and the final estimation step. Normally, a guided filter with a larger filtering window can better reduce the speckle, while a filter with a smaller window can better retain the image details. In this research, we propose an adaptive strategy for setting the sizes of the filtering windows, based on the local homogeneity of the image.

Before the filtering, we divide all of the 7×7 image patches into three different types, namely, homogeneous areas, moderately homogeneous areas, and heterogeneous areas. This approach is accomplished by the method proposed in [30]: a patch can be regarded as a homogeneous one if STM $<=$ $((4/\pi - 1)/L)^{1/2}$, where STM

denotes the standard deviation to the mean of the total intensity of the patch and L denotes the number of looks, while a patch can be regarded as a heterogeneous one if STM $>= \sqrt{3}\cdot((4/\pi - 1)/L)^{1/2}$; otherwise, it is a moderately homogeneous patch. Therefore, to better reduce the speckle in the homogeneous areas and preserve the edges in the heterogeneous areas, the size of Δx or Δi can be set as 9×9, 7×7, or 5×5, according to the homogeneity of the corresponding 7×7 patch when despeckling a certain pixel.

The filtering procedure of the proposed PNGF method can be summarized as follows.

1) The standard deviation to the mean of the total intensity of each 7×7 image patch is calculated.
2) Parameter $t1$ in the weight kernel of (15) is determined by the aforementioned "noise estimator."
3) For each pixel in the image, its basic estimation is calculated by (14) and (15), where the size of Δx is determined based on the homogeneity of its local 7×7 patch obtained in step 1.
4) Parameter $t2$ in the weight kernel of (16) is also determined by the "noise estimator."
5) For each pixel in the image, the final estimation is calculated by (13) and (16), where the size of Δi is also determined based on the homogeneity of its local 7×7 patch obtained in step 1.

IV. Experimental Part

In this section, to illustrate the filtering performance of the proposed PNGF method, the results obtained with a simulated PolSAR image and two real PolSAR images are reported. The source code of the proposed PNGF method can be downloaded from the link (http://sendimage.whu.edu.cn/en/resources/). Three state-of-the-art PolSAR filters were also implemented for comparison purposes: the NL-SAR filter [14], the PolSAR nonlocal total variation (NLTV) filter [19], and the PolSAR SSC filter [21]. All of these three methods were implemented by the source codes or tools provided by the authors of the respective papers.

To quantitatively evaluate the filtering performances of different methods, the equivalent number of looks (ENL), the edge-preservation degree based on the ratio of average (EPD-ROA) [31], and the target-to-clutter ratio (TCR) are employed [32].

The ENL is an important indicator to assess the amount of speckle in SAR images, and is generally computed as

$$\mathrm{ENL} = 1/\sigma_v^2 \tag{23}$$

where σ_v denotes the coefficient of variation of the intensity inhomogeneous areas. A higher ENL value indicates a better speckle reduction result.

The EPD-ROA indicator is given by

$$\text{EPD-ROA} = \frac{\sum_{i=1}^{N} |I_{d1}(i)/I_{d2}(i)|}{\sum_{i=1}^{N} |I_{s1}(i)/I_{s2}(i)|} \tag{24}$$

where I_{d1} and I_{d2} denote the adjacent pixel values of the despeckled image along a certain direction, respectively. Similarly, I_{s1} and I_{s2} denote the corresponding adjacent pixel values of the speckled image. An EPD-ROA value closer to one indicates better edge-preservation ability.

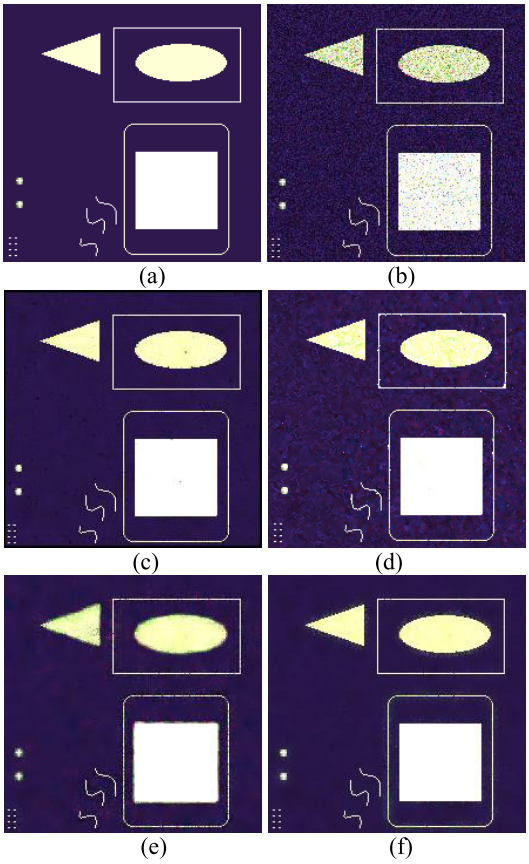

Fig. 1. Filtering results for the simulated image. (a) Reference image. (b) Speckled image. Despeckling results of (c) NL-SAR filter, (d) PolSAR NLTV method, (e) PolSAR SSC method, and (f) proposed PNGF method.

The TCR indicator measures the difference in the intensity ratios between the point targets and the surrounding areas before and after despeckling by

$$\mathrm{TCR} = \left| 20\log_{10}\frac{\max_p(I_d)}{\mathrm{mean}_p(I_d)} - 20\log_{10}\frac{\max_p(I_s)}{\mathrm{mean}_p(I_s)} \right| \tag{25}$$

where I_s and I_d are, respectively, the speckled intensity image and the despeckled intensity image. Subscript p denotes the patch containing a point target, and $\max_p$ and mean_p are computed over the patch. Since the speckle model does not hold in the presence of persistent scatterers or point targets, a low TCR value indicates that the filter effectively preserves their original signatures.

A. Experiments With a Simulated PolSAR Image

In this paper, a single-look simulated PolSAR image [Fig. 1(b)], which was obtained by the procedure based on Monte Carlo simulation [24], was used to compare the filtering performances of different methods. The image contains linear and nonlinear edges, and high returns from point signatures. Table I shows the quantitative assessment results of different methods on this image.

As can be observed in Fig. 1, at first sight, the NL-SAR filter and the proposed PNGF show quite comparable results: the

TABLE I

QUANTITATIVE ASSESSMENT RESULTS FOR THE SIMULATED IMAGES FILTERED BY DIFFERENT METHODS

	ENL	TCR	EPD-ROA
NL-SAR	35.4	3.83	0.82
PolSAR NLTV	15.4	5.88	0.89
PolSAR SSC	24.1	6.61	0.68
PNGF	35.7	4.04	0.83

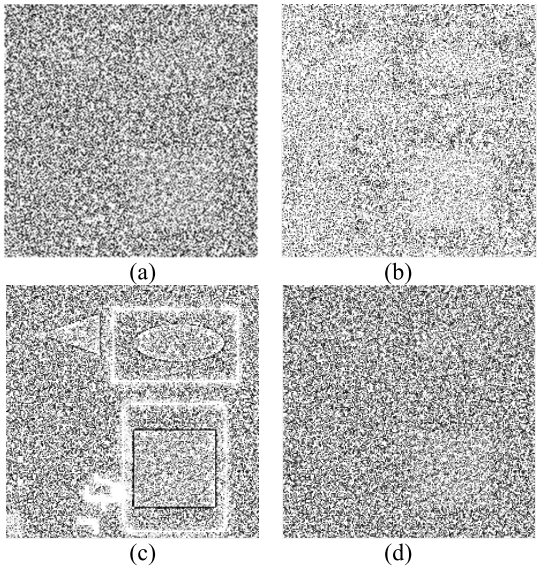

Fig. 2. Ratio images for (a) NL-SAR filter, (b) PolSAR NLTV filter, (c) PolSAR SSC filter, and (d) proposed method.

speckle is notably reduced and the edges are well preserved, which can also be seen in the ENL values and EPD-ROA values in Table I. However, one can also observe that some dark speckle still resides on the bright areas of the image filtered by the NL-SAR filter. For the PolSAR NLTV filter, the high value of EPD-ROA reveals its good performance in retaining edges. However, visually, this despeckling method does not significantly reduce the speckle, which can also be seen by its low ENL value. Visually, the PolSAR SSC filter shows a good performance in suppressing speckle. However, the filtered image [Fig. 1(e)] appears to be over-smoothed and shows a partial halo effect.

To further validate the capability of different techniques in retaining edges, we show the ratio images in Fig. 2 between the noisy intensity image and the despeckled intensity images. Theoretically, for an ideal filter, the ratio image should be pure speckle. It can be seen that the ratio images for the NL-SAR filter, the PolSAR NLTV filter, and the proposed PNGF method have the appearance of random noise, while the edges are notably retained in the ratio image for the PolSAR SSC filter, which indicates that PolSAR SSC is not very good in retaining edges and is consistent with the conclusion one can draw from the EPD-ROA values.

B. Experiments With Two Real PolSAR Images

Two real PolSAR images were used to validate the effectiveness of the proposed despeckling method. Both of the images were acquired by the AIRSAR project of the National Aeronautics and Space Administration/Jet Propulsion Laboratory, and were processed by the European Space Agency as four-look data sets.

TABLE II

QUANTITATIVE ASSESSMENT RESULTS FOR THE REAL POLSAR DATA SETS FILTERED BY DIFFERENT METHODS

	Kyoto image			San Francisco image		
	ENL	TCR	EPD-ROA	ENL	TCR	EPD-ROA
NL-SAR	74.0	5.03	0.725	60.2	2.88	0.819
PolSAR NLTV	33.3	4.04	0.814	21.2	3.30	0.824
PolSAR SSC	66.9	9.12	0.730	59.1	2.12	0.805
PNGF	42.3	3.69	0.788	34.7	2.22	0.760

1) Experiments on the Kyoto Image: The first real PolSAR image used for the comparison was a C-band AIRSAR image acquired in Kyoto, Japan [Fig. 3(a)]. At first sight, the NL-SAR filter and the PolSAR SSC filter show the over-smoothing problem, especially in the forest and urban areas. In contrast, the PolSAR NLTV method and the PNGF method effectively retain most of the details exhibited in these areas. The above observations can also be confirmed by the EPD-ROA and TCR values listed in Table II, although the ENL values reveal that the NLM filter and the SSC filter reduce the speckle to much larger extents. To further reveal the over-smoothing problem of the NL-SAR filter and the PolSAR SSC filter, we display the ratio images of different filters on this data set in Fig. 4. Clearly, compared with the PolSAR NLTV filter and the PNGF filter, the other two filters, especially the NL-SAR filter, filter out much more details from the original image.

Some other phenomena can also be observed in Fig. 3. First, the PolSAR NLTV method seems to distort the polarimetric scattering mechanisms of the image, which changes the color of the Pauli RGB composite image to some degree. In fact, the radiometric distortion problem of this method was also reported in [1]. Second, some artifacts can be found in the PolSAR SSC filtered image, especially for some strong returns in the urban areas [marked by the red arrow in Fig. 3(i)]

PolSAR image despeckling is an open issue. In a sense, choosing a proper filter is application oriented. As an important preprocessing step before using PolSAR data to extract land-object information, a robust despeckling algorithm should not only effectively suppress the speckle and retain the edges, but also enhance the differences between the classes and preserve the polarimetric scattering mechanisms. To inspect the general performances of different filters with regard to the aforementioned issues, we provide scattergrams of the Cloude polarimetric decomposition parameters (entropy H, anisotropy A, and alpha angle α) [33] in Fig. 5 for three areas with different land-object types, as marked in Fig. 3(a). The polarimetric scattering entropy is an index used to describe the degree of statistical disorder of each distinct scatter type within the ensemble (i.e., the randomness of the scattering); the polarimetric scattering anisotropy measures the relative importance of the second and the third eigenvalues of the eigen

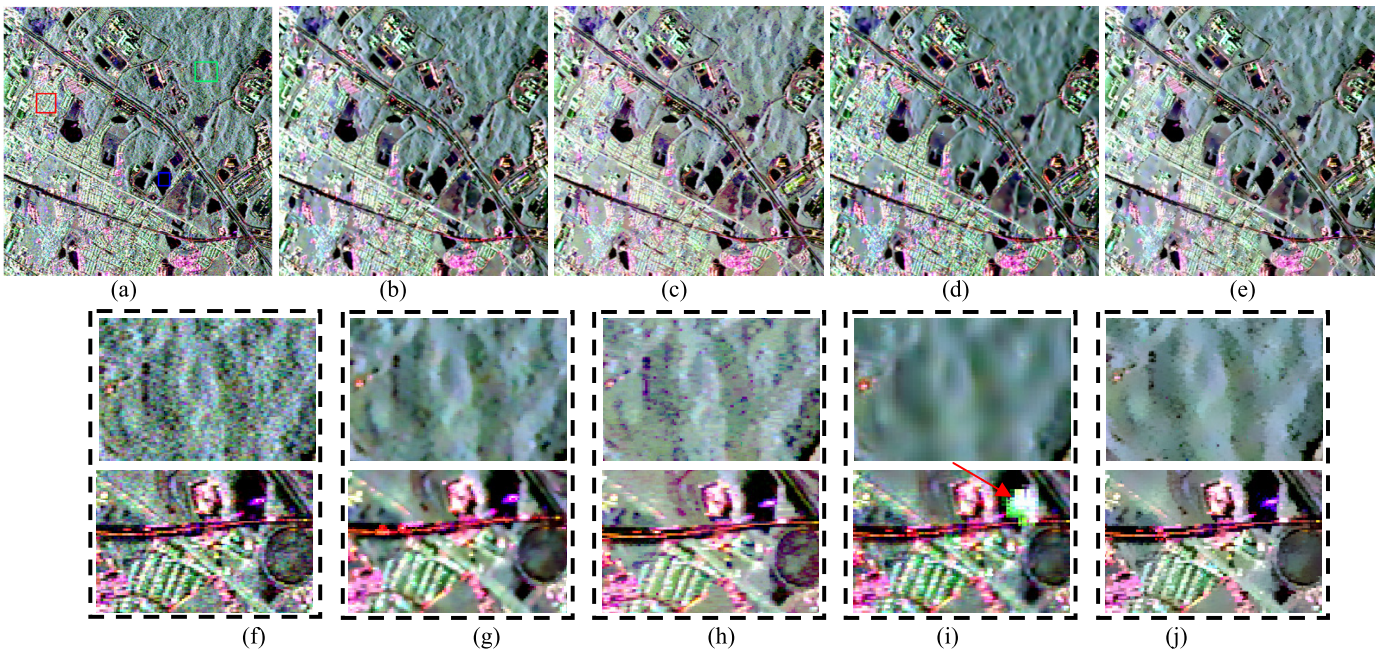

Fig. 3. Filtering results for the Kyoto image. (a) Pauli RGB image of the speckled data. Filtering results of (b) NL-SAR filter, (c) PolSAR NLTV method, (d) PolSAR SSC method, and (e) PNGF method. (f)–(j) Subimages cropped from (a)–(e), respectively.

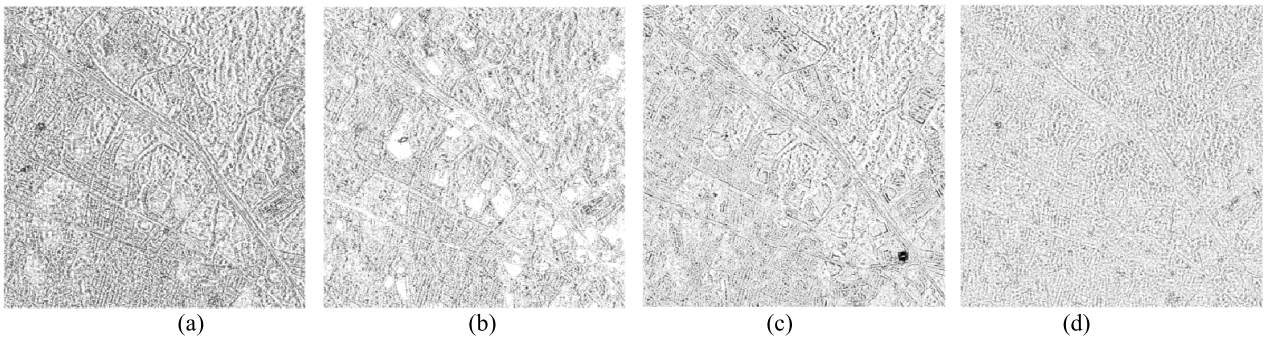

Fig. 4. Ratio images of the Kyoto image filtered by (a) NL-SAR filter, (b) PolSAR NLTV filter, (c) PolSAR SSC filter, and (d) proposed PNGF method.

decomposition; the alpha angle is related to underlying average physical scattering mechanism.

First of all, the objects are much more separable for the filtered data than for the original data, due to the suppression of the speckle. Second, the distribution of the parameters in the image processed by the PolSAR NLTV method [Fig. 5(c)] shows a notable shift from the speckled data, which demonstrates the radiometric distortion problem we observed before. It is also interesting to note that compared with the highly concentrated water pixels in the PNGF-filtered image, the pixels of the other two land-object types are much more dispersed. This is because the scattering mechanisms of forest on the mountains and buildings in the urban areas are often very complicated. The proposed method retains different scattering mechanisms that these two areas intrinsically possess.

2) Experiments on the San Francisco Image: The filtering results of different methods on the L-band San Francisco image are shown in Fig. 6. Once again, the PolSAR NLTV filter does not effectively suppress the speckle, although it performs the best in preserving edges among the four methods, which can be confirmed from both the visual observation and quantitative indicators. The PolSAR SSC filter again shows a partial halo effect, which slightly degrades the spatial resolution of the image. Visually, the NL-SAR filter and the PNGF filter produce good balance between reducing speckle and retaining image spatial resolution. Relative speaking, the NL-SAR filter reduce the speckle to a larger degree, while the PNGF filter better preserves the details.

For many applications, such as ship and man-made structure detection, maintaining the signatures of these targets is important. Furthermore, unlike the scattering from distributed media, the scattering from point targets comes mainly from a few strong scatterers within a resolution cell, and it is better to maintain their original polarimetric information. To validate the capability of the despeckling methods in maintaining the polarimetric traits of point targets, we chose one of the targets on the sea, as marked in Fig. 6(a), and plotted its cross-polarization signature (Fig. 7) for each filtered image. Clearly, distinct disagreements arise between the signatures from the original pixel and the pixels processed by the PolSAR NLTV filter, while much closer agreements are reached for the targets processed by the other three methods.

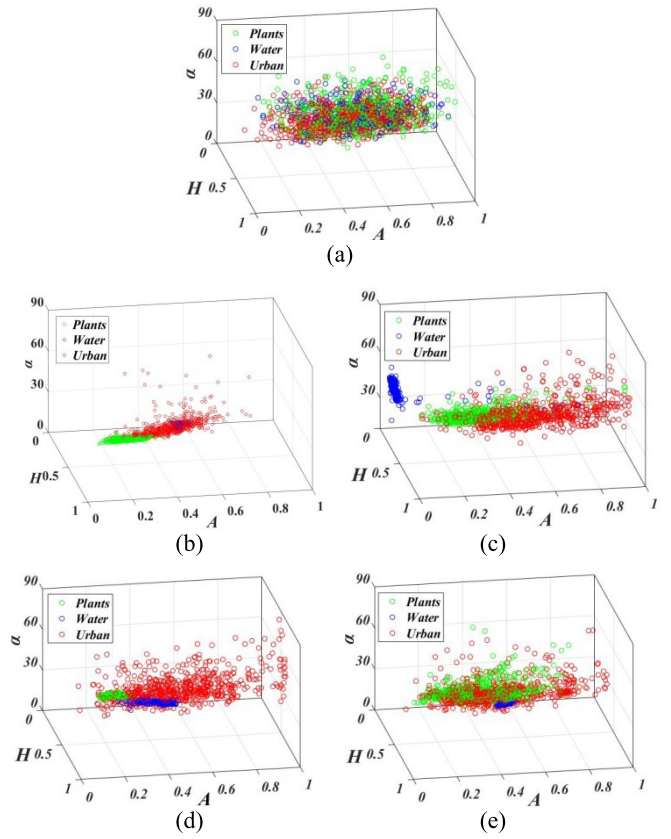

Fig. 5. Scattergrams of the Cloude polarimetric decomposition parameters for different areas in (a) speckled image, and (b)–(e) NL-SAR filter, the PolSAR NLTV method, the PolSAR SSC method, and the PNGF method, respectively.

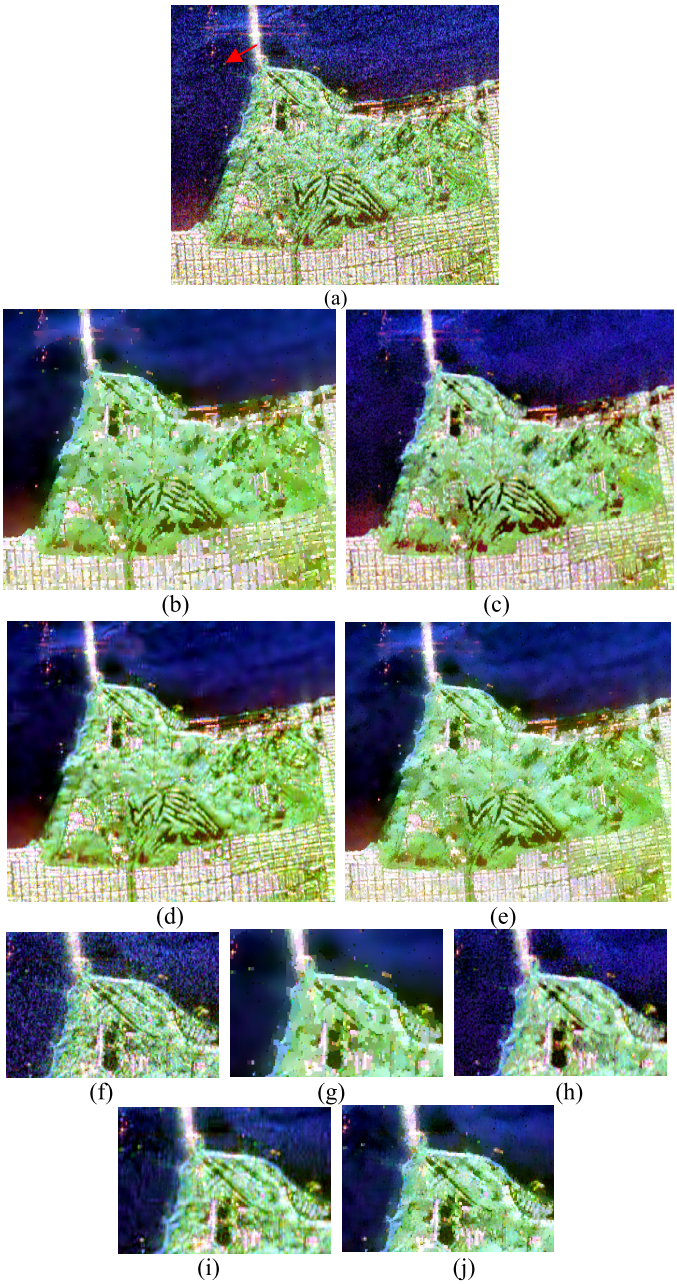

Fig. 6. Filtering results for the San Francisco image. (a) Pauli RGB image of the speckled data. Filtering results of (b) NL-SAR filter, (c) PolSAR NLTV method, (d) PolSAR SSC method, and (e) PNGF method, respectively. (f)–(j) Subimages cropped from (a)–(e), respectively.

C. Computational Complexity

As reviewed in [1], many newly developed PolSAR despeckling methods are nonlocal patch based or globally collaborative algorithms, and high computational complexity is often one of the main issues for their wide application. Furthermore, for many of the new SAR systems, such as the Chinese GF-3 system, their image dimensions can be higher than $10\,000 \times 10\,000$ pixels. It is therefore a challenge to develop a PolSAR filtering algorithm which can balance the computational efficiency and the despeckling effectiveness. Although it is difficult to directly compare the computational times of the method presented in this paper and the other three state-of-the-art methods, since they were implemented on different platforms, we can qualitatively analyze and compare their computational complexity.

We assume that the size of the image is $m \times n$ and, in the three state-of-the-art methods, the search window size is $w_1 \times w_1$ (often larger than 11×11) and the target patch size is $w_2 \times w_2$.

1) We let the similarity measure between two pixels be one step, and it can thus be concluded that the complexity of the NL-SAR filter is about $O(mnw_1^2w_2^2)$.
2) For the PolSAR NLTV filter, as per the deduction in [19], the complexity is about $O(mnw_1^2w_2^2 + mnIr)$, where I is the iteration times of the filter and r is the number of selected nearest neighbors in the search area.
3) For the PolSAR SSC filter, it has been deduced [1] that its total computational complexity is slightly lower than that of the NLM filter if the sliding step in the patch ordering procedure is set as two.
4) For the proposed PNGF method, there are two filtering steps—the prefiltering step and the final filtering step—for which the averaging window sizes are both nearly 7×7 for most images. We have also found that the computational time of the similarity measure between two pixels in the final step is about two times that in the prefiltering step. Therefore, based on the fact that the similarity measure in the first step can be

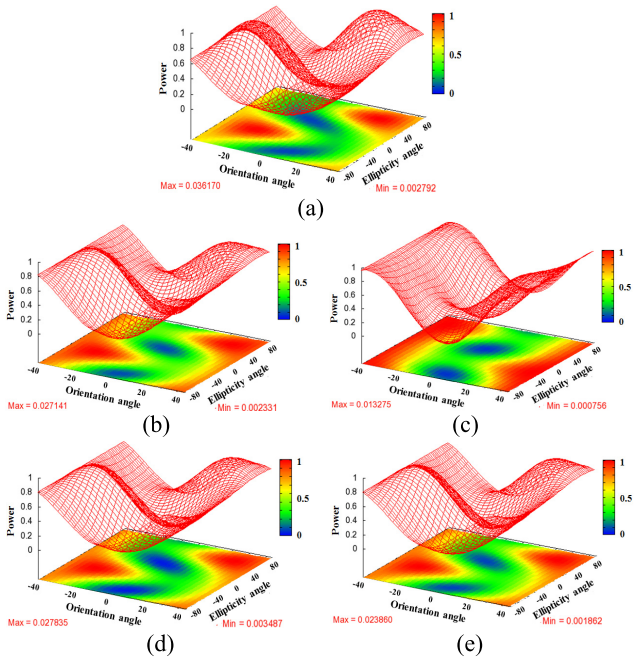

Fig. 7. Cross-polarization signatures of a point target in different images. (a) Original cross-polarization signature of the target. (b)–(e) Cross-polarization signature of the target in the images filtered by the NL-SAR filter, the PolSAR NLTV method, the PolSAR SSC method, and the PNGF method, respectively.

directly employed in the final step, we can conclude that the computational complexity of the proposed method is nearly $O(2 \times 7^2 \times mn)$. To sum up, we can conclude from the above analyses that the PNGF method is much more computationally efficient than the three state-of-the-art methods compared in this paper.

V. Conclusion

Despeckling is a fundamental preprocessing step for applications using PolSAR data in most cases. Recent years have shown a rapid development in the designing of PolSAR filtering algorithms, especially those nonlocal patch-based filters. Although most of these filters can obtain good results in many cases, the high computational burden may hamper their practical application, particularly for the newly launched space-borne PolSAR systems with large image sizes. It is a challenge to develop a PolSAR filtering algorithm which can balance the computational efficiency and the despeckling effectiveness.

In this paper, we have presented a guided filter with nonlinear weight kernels and adaptive filtering windows for PolSAR image despeckling. The PNGF consists of two main steps: 1) in the first step, a guidance image with a relatively low level of speckle is constructed by a local weighted average using the statistical trait of the speckled data and 2) in the second step, the final output image is obtained with the aid of the fully polarimetric traits from both the guidance image and the speckled image. Experiments conducted on both simulated and real PolSAR data sets confirm the promising performance of the proposed method, both in reducing speckle and retaining image details. In addition, the low computational complexity is another strength of the proposed method when compared with some of the nonlocal patch based or globally collaborative despeckling algorithms.

References

[1] X. Ma, P. Wu, Y. Wu, and H. Shen, "A review on recent developments in fully polarimetric SAR image despeckling," *IEEE J. Sel. Topics Appl. Earth Observ. Remote Sens.*, vol. 11, no. 3, pp. 743–758, Mar. 2018, doi: 10.1109/JSTARS.2017.2768059.

[2] J.-S. Lee, M. R. Grunes, and G. de Grandi, "Polarimetric SAR speckle filtering and its implication for classification," *IEEE Trans. Geosci. Remote Sens.*, vol. 37, no. 5, pp. 2363–2373, Sep. 1999.

[3] J.-S. Lee, "Digital image enhancement and noise filtering by use of local statistics," *IEEE Trans. Pattern Anal. Mach. Intell.*, vol. PAMI-2, no. 2, pp. 165–168, Mar. 1980.

[4] J.-S. Lee, M. R. Grunes, D. L. Schuler, E. Pottier, and L. Ferro-Famil, "Scattering-model-based speckle filtering of polarimetric SAR data," *IEEE Trans. Geosci. Remote Sens.*, vol. 44, no. 1, pp. 176–187, Jan. 2006.

[5] G. Vasile, E. Trouve, J.-S. Lee, and V. Buzuloiu, "Intensity-driven adaptive-neighborhood technique for polarimetric and interferometric SAR parameters estimation," *IEEE Trans. Geosci. Remote Sens.*, vol. 44, no. 6, pp. 1609–1621, Jun. 2006.

[6] J.-S. Lee, J.-H. Wen, T. L. Ainsworth, K.-S. Chen, and A. J. Chen, "Improved sigma filter for speckle filtering of SAR imagery," *IEEE Trans. Geosci. Remote Sens.*, vol. 47, no. 1, pp. 202–213, Jan. 2009.

[7] J.-S. Lee, "A simple speckle smoothing algorithm for synthetic aperture radar images," *IEEE Trans. Syst., Man, Cybern.*, vol. SMC-13, no. 1, pp. 85–89, Jan./Feb. 1983.

[8] J.-S. Lee, T. L. Ainsworth, Y. Wang, and K.-S. Chen, "Polarimetric SAR speckle filtering and the extended sigma filter," *IEEE Trans. Geosci. Remote Sens.*, vol. 53, no. 3, pp. 1150–1160, Mar. 2015.

[9] A. Alonso-González, C. López-Martínez, and P. Salembier, "Filtering and segmentation of polarimetric SAR data based on binary partition trees," *IEEE Trans. Geosci. Remote Sens.*, vol. 50, no. 2, pp. 593–605, Feb. 2012.

[10] O. D'Hondt, S. Guillaso, and O. Hellwich, "Iterative bilateral filtering of polarimetric SAR data," *IEEE J. Sel. Topics Appl. Earth Observ. Remote Sens.*, vol. 6, no. 3, pp. 1628–1639, Jun. 2013.

[11] C. López-Martínez and X. Fabregas, "Model-based polarimetric SAR speckle filter," *IEEE Trans. Geosci. Remote Sens.*, vol. 46, no. 11, pp. 3894–3907, Nov. 2008.

[12] J. Chen, Y. Chen, W. An, Y. Cui, and J. Yang, "Nonlocal filtering for polarimetric SAR data: A pretest approach," *IEEE Trans. Geosci. Remote Sens.*, vol. 49, no. 5, pp. 1744–1754, May 2011.

[13] H. Zhong, J. Zhang, and G. Liu, "Robust polarimetric SAR despeckling based on nonlocal means and distributed Lee filter," *IEEE Trans. Geosci. Remote Sens.*, vol. 42, no. 7, pp. 4198–4210, Jul. 2014.

[14] C.-A. Deledalle, L. Denis, F. Tupin, A. Reigber, and M. Jäger, "NL-SAR: A unified nonlocal framework for resolution-preserving (Pol)(In)SAR denoising," *IEEE Trans. Geosci. Remote Sens.*, vol. 53, no. 4, pp. 2021–2038, Apr. 2015.

[15] A. Buades, B. Coll, and J.-M. Morel, "A non-local algorithm for image denoising," in *Proc. IEEE Comput. Soc. Conf. Comput. Vis. Pattern Recognit.*, vol. 2, Jun. 2005, pp. 60–65.

[16] X. Ma, H. Shen, L. Zhang, J. Yang, and H. Zhang, "Adaptive anisotropic diffusion method for polarimetric SAR speckle filtering," *IEEE J. Sel. Topics Appl. Earth Observ. Remote Sens.*, vol. 8, no. 3, pp. 1041–1050, Mar. 2015.

[17] X. Ma, H. Shen, and L. Zhang, "PolSAR anisotropic diffusion filter with a refined similarity measure and an adaptive fidelity constraint," *Int. J. Remote Sens.*, vol. 37, no. 24, pp. 5988–6011, 2016.

[18] X. Nie, H. Qiao, and B. Zhang, "A variational model for PolSAR data speckle reduction based on the wishart distribution," *IEEE Trans. Image Process.*, vol. 24, no. 4, pp. 1209–1222, Apr. 2015.

[19] X. Nie, H. Qiao, B. Zhang, and X. Huang, "A nonlocal TV-based variational method for PolSAR data speckle reduction," *IEEE Trans. Image Process.*, vol. 25, no. 6, pp. 2620–2634, Jun. 2016.

[20] X. Ma, H. Shen, X. Zhao, and L. Zhang, "SAR image despeckling by the use of variational methods with adaptive nonlocal functionals," *IEEE Trans. Geosci. Remote Sens.*, vol. 54, no. 6, pp. 3421–3434, Jun. 2016.

[21] B. Xu, Y. Cui, B. Zuo, J. Yang, and J. Song, "Polarimetric SAR image filtering based on patch ordering and simultaneous sparse coding," *IEEE Trans. Image Process.*, vol. 54, no. 7, pp. 4079–4093, Jul. 2016.

[22] K. He, J. Sun, and X. Tang, "Guided image filtering," *IEEE Trans. Pattern Anal. Mach. Intell.*, vol. 35, no. 6, pp. 1397–1409, Jun. 2013.
[23] W. Ni and X. Gao, "Despeckling of SAR image using generalized guided filter with Bayesian nonlocal means," *IEEE Trans. Geosci. Remote Sens.*, vol. 54, no. 1, pp. 567–579, Jan. 2016.
[24] J.-S. Lee and E. Pottier, *Polarimetric Radar Imaging: From Basics to Applications*. Boca Raton, FL, USA: CRC Press, 2009.
[25] N. R. Goodman, "Statistical analysis based on a certain multivariate complex Gaussian distribution (an introduction)," *Ann. Math. Statist.*, vol. 34, no. 1, pp. 152–177, 1963.
[26] C. López-Martínez and X. Fabregas, "Polarimetric SAR speckle noise model," *IEEE Trans. Geosci. Remote Sens.*, vol. 41, no. 10, pp. 2232–2242, Oct. 2003.
[27] T. Hastie, R. Tibshirani, and J. H. Friedman, *The Elements of Statistical Learning*. Berlin, Germany: Springer, 2003.
[28] K. Conradsen, A. A. Nielsen, J. Schou, and H. Skriver, "A test statistic in the complex Wishart distribution and its application to change detection in polarimetric SAR data," *IEEE Trans. Geosci. Remote Sens.*, vol. 41, no. 1, pp. 4–19, Jan. 2003.
[29] J. Canny, "A computational approach to edge detection," *IEEE Trans. Pattern Anal. Mach. Intell.*, vol. PAMI-8, no. 6, pp. 679–698, Nov. 1986.
[30] A. Lopes, R. Touzi, and E. Nezry, "Adaptive speckle filters and scene heterogeneity," *IEEE Trans. Geosci. Remote Sens.*, vol. 28, no. 6, pp. 992–1000, Nov. 1990.
[31] H. Feng, B. Hou, and M. Gong, "SAR image despeckling based on local homogeneous-region segmentation by using pixel-relativity measurement," *IEEE Trans. Geosci. Remote Sens.*, vol. 49, no. 7, pp. 2724–2737, Jul. 2011.
[32] F. Argenti, A. Lapini, T. Bianchi, and L. Alparone, "A tutorial on speckle reduction in synthetic aperture radar images," *IEEE Geosci. Remote Sens. Mag.*, vol. 1, no. 3, pp. 6–35, Sep. 2013.
[33] S. R. Cloude and E. Pottier, "An entropy based classification scheme for land applications of polarimetric SAR," *IEEE Trans. Geosci. Remote Sens.*, vol. 35, no. 1, pp. 68–78, Jan. 1997.

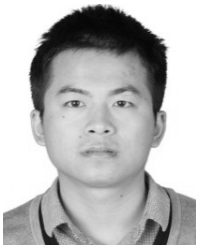

Xiaoshuang Ma received the B.S. degree in geographic information system from Hubei University, Wuhan, China, in 2011, and the Ph.D. degree in cartography and geographic Information engineering from Wuhan University, Wuhan, in 2016.

He is currently a Lecturer with the Department of Resources and Environmental Engineering, Anhui University, Hefei, China. His research interests include synthetic aperture radar image processing and interpretation.

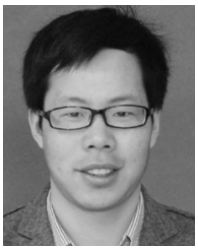

Penghai Wu (M'16) received the B.S. degree in environmental science from Anqing Normal College, Anqing, China, in 2009, and the M.S. degree in surveying and mapping engineering and the Ph.D. degree in cartography and geographical information engineering from Wuhan University, Wuhan, China, in 2011 and 2014, respectively.

He is currently an Associate Professor with the School of Resources and Environmental Engineering, Anhui University, Hefei. He has authored over 20 research papers published in journals, such as the *Remote Sensing of Environment* and the IEEE TRANSACTIONS ON GEOSCIENCE AND REMOTE SENSING. His research interests include spatiotemporal fusion, the disaggregation of land surface temperature, the reconstruction of land surface temperature, and regional ecoenvironmental change.

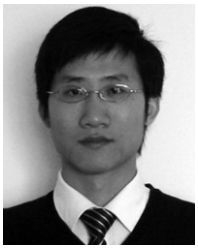

Huanfeng Shen (M'10–SM'13) received the B.S. degree in surveying and mapping engineering and the Ph.D. degree in photogrammetry and remote sensing from Wuhan University, Wuhan, China, in 2002 and 2007, respectively.

In 2007, he joined the School of Resource and Environmental Sciences, Wuhan University, where he is currently a Luojia Distinguished Professor. He has authored over 100 research papers. His research interests include image quality improvement, remote-sensing mapping and application, data fusion and assimilation, and regional and global environmental change.

Dr. Shen is currently a member of the Editorial Board of the *Journal of Applied Remote Sensing*. He has been supported by several talent programs, such as the Youth Talent Support Program of China in 2015, the China National Science Fund for Excellent Young Scholars in 2014, and the New Century Excellent Talents by the Ministry of Education of China in 2011.